Role of charge saturation in photorefractive dynamics of micron-sized beams and departure from soliton behavior

E. DelRe,[1,2,*] A. Ciattoni,[2,3] and E. Palange[1,2]

[1]*Laboratorio di Ottica e Fotonica, Dipartimento di Ingegneria Elettrica, Università dell'Aquila, Monteluco di Roio 67040 L'Aquila, Italy*

[2]*Instituto Nazionale per la Fisica della Materia, Consiglio Nazionale delle Ricerche, 67040 L'Aquila, Italy*

[3]*Dipartimento di Fisica, Università dell'Aquila, 67010 L'Aquila, Italy*

(Received 7 October 2005; published 30 January 2006)

Experimental and theoretical results indicate that miniaturized micron-sized nonlinear beam phenomenology in photorefractives leads to a regime qualitatively distinct from solitonlike propagation on consequence of the specific role of space-charge saturation. In the highly modulated conditions typical of beams, this contribution amounts to an effective electron self-action.

DOI: 10.1103/PhysRevE.73.017601 PACS number(s): 42.65.Tg, 42.70.−a

Light beams propagating in photorefractive material experience a nonlinearity that leads to startling and useful phenomenology even for low intensity regimes [1]. Optical self-action is associated to the alteration of beam propagation due to local light-driven electro-optic changes in the material index of refraction. These are produced by the electric space-charge field generated by the charges displaced from photoionized impurity sites. The effect is sensitive to the beam transverse shape and to the presence of external applied electric fields, these determining the charge transport processes. In the absence of bias, charge movement is triggered by diffusion that can mediate two-wave-mixing for plane waves, fanning for beams that have a relatively large waist [1], or anisotropic self-focusing for confined beams in paraelectric crystals [2]. When bias is applied, diffusion combines with charge drift and solitons can be observed, self-action resulting in a distributed self-lensing effect that exactly balances diffraction, both in a transient (or quasi-steady-state) [3] and in a steady-state regime [4] (for a review see Ref. [5]). This occurs in a slowly varying condition in which the transverse beam features are large enough to make diffusion and other mechanisms, such as charge saturation, amount to small perturbations. In this regime, in a reduced 1+1D (one-transverse-and-one-propagation-dimension) condition, soliton size turns out to have no physical role, simply scaling the required nonlinear response: tighter solitons require a stronger external biasing electric field E_0. In the transient, this finding is supported by numerical simulation of experiments [6], whereas in the steady state, this is underlined by the emergence of an effective Kerr-saturated nonlinearity [7]. Furthermore, whereas for more confined beams (down to 10 μm) charge diffusion and partial charge saturation do increase, these simply slant or self-bend the soliton trajectory in a manner that now explicitly depends on its size [8].

Since experiments typically involve beams with widths of the order of 10 μm or wider, this picture holds for the greater part of reported observations for 1+1D solitons [3,4], and even in part for the more complex 2+1D solitons [9,10]. In turn, recent developments have involved considerably smaller beam and/or soliton sizes, of the order of a few microns, especially in connection with optimal single-mode fiber-soliton coupling [11]. In comparison to previous literature, results indicated a series of qualitatively new phenomena, which included what appeared to be a temporal succession of different "soliton stages." The fact that standard soliton models did not predict this behavior suggested that the small size of input launch beam could activate photorefractive mechanisms excluded by conventional approximation schemes. The aim of this present study is to extend investigation to this highly confined case for 1+1D beams. We will find that the micron-sized transverse features now involve charge saturation in a nontrivial way, implying a generalization of the standard material response model to include all the principal mechanisms of the photorefractive band-transport model. Apart from providing an understanding of observed phenomenology, this study can become central in identifying the ultimate limits to the transverse miniaturization of screening solitons, influencing passive, nonlinear, and electro-optical soliton-based device design [12]. It can be furthermore instrumental in the elaboration of a scheme for the future investigation of even tighter beam evolution, where nonlinear electromagnetic nonparaxial soliton mechanisms, presently identified in Kerr media, could be observed through photorefractive self-action [13].

In order to identify and compare the basic physical mechanisms participating in the material response and consequently implement an efficient simulation strategy, it is convenient to make use of an appropriate approximate relationship between the optical intensity I and the space-charge field $\mathbf{E}$. In the generally adopted approximation, valid for propagation of beams with scales of the order of 10 μm or more, the relationship between I and $\mathbf{E}$ is obtained from the equation [5,14]

$$\nabla \cdot \left[\tau \frac{\partial \mathbf{E}}{\partial t} + \mathbf{E}N + \frac{k_b T}{q} \nabla N \right] = 0, \quad (1)$$

with

*Electronic address: edelre@ing.univaq.it

$$N = Q\frac{1 - \dfrac{\epsilon\nabla \cdot \mathbf{E}}{\alpha N_a q}}{1 + \dfrac{\epsilon\nabla \cdot \mathbf{E}}{N_a q}}, \qquad (2)$$

and the time scale $\tau=\gamma\epsilon/q\mu s\alpha I_d$, γ is the electron recombination rate, q the electron charge, ϵ the dielectric constant, μ the charge mobility, s the photoexcitation cross section, $\alpha=(N_d-N_a)/N_a$ ($\gg 1$) the ratio of donor and acceptor concentration, $I_d=\beta/s$ the so-called dark illumination, β the thermal excitation rate, and $Q=1+I/I_d$. We have singled out Eq. (2), which provides the relationship of the normalized conduction band electron density to I and $\mathbf{E}$ [$N\equiv\gamma N_e/(\alpha\beta)$, where N_e is the electron concentration] from Eq. (1) because, as we shall discuss below, the critical approximations relevant to tight beams involve specifically the expression in Eq. (2). Equations (1) and (2) are generally further simplified in the slowly varying approximation, for which both $|(\varepsilon/qN_a)\nabla\cdot\mathbf{E}|\ll 1$ and $|(k_bT/E_0q)\boldsymbol{\nabla}\ln(I+I_d)|\ll 1$, and the zero-order steady-state response $\nabla\cdot[\mathbf{E}(1+I/I_d)]=0$ in a 1+1D geometry leads to a local Kerr-saturated nonlinearity $\Delta n\propto 1/(1+I/I_d)^m$ ($m=1,2$ for ferroelectric and paraelectrics, respectively) [4,15]. Equation (2) [and consequently Eq. (1)] becomes singular and unphysical when $\boldsymbol{\nabla}\cdot\mathbf{E}\simeq -qN_a/\varepsilon$. For a beam this occurs when its transverse spatial scale is comparable with $\ell_{\rm lim}$ determined by the condition that the optically induced electric field reaches, at some instant and in a given region, what is generally termed the saturation field, $E\sim(N_aq/\varepsilon)\ell_{\rm lim}\equiv E_{\rm sat}$ [1]. This typically implies, for a given steady-state soliton, an $\ell_{\rm lim}$ of the order of a few microns. For example, in a ferroelectric strontium-barium-niobate with $\varepsilon=10^3\varepsilon_0$, $N_a=2\times10^{22}$ m^{-3}, index of refraction of $n=2.5$, and a linear electro-optic coefficient $r=200$ pm/V, $\ell_{\rm lim}\sim 3$ μm for a $\lambda=0.5$ μm screening soliton of intensity ratio $u_0^2=I_p/I_d=(4)^2$, where I_p is the peak beam intensity I_p [7]. Similarly, for a sample of paraelectric potassium-lithium-tantalate-niobate (KLTN) with $\varepsilon=10^4\varepsilon_0$ and a quadratic electro-optic coefficient $g=0.12$ m^2 C^{-4}, the limiting beam width in the same conditions for steady-state screening solitons is $\ell_{\rm lim}\sim 6$ μm (actually, in this case the condition turns out to be independent of ε) [15].

To observe optical propagation when Eq. (1) [with condi-

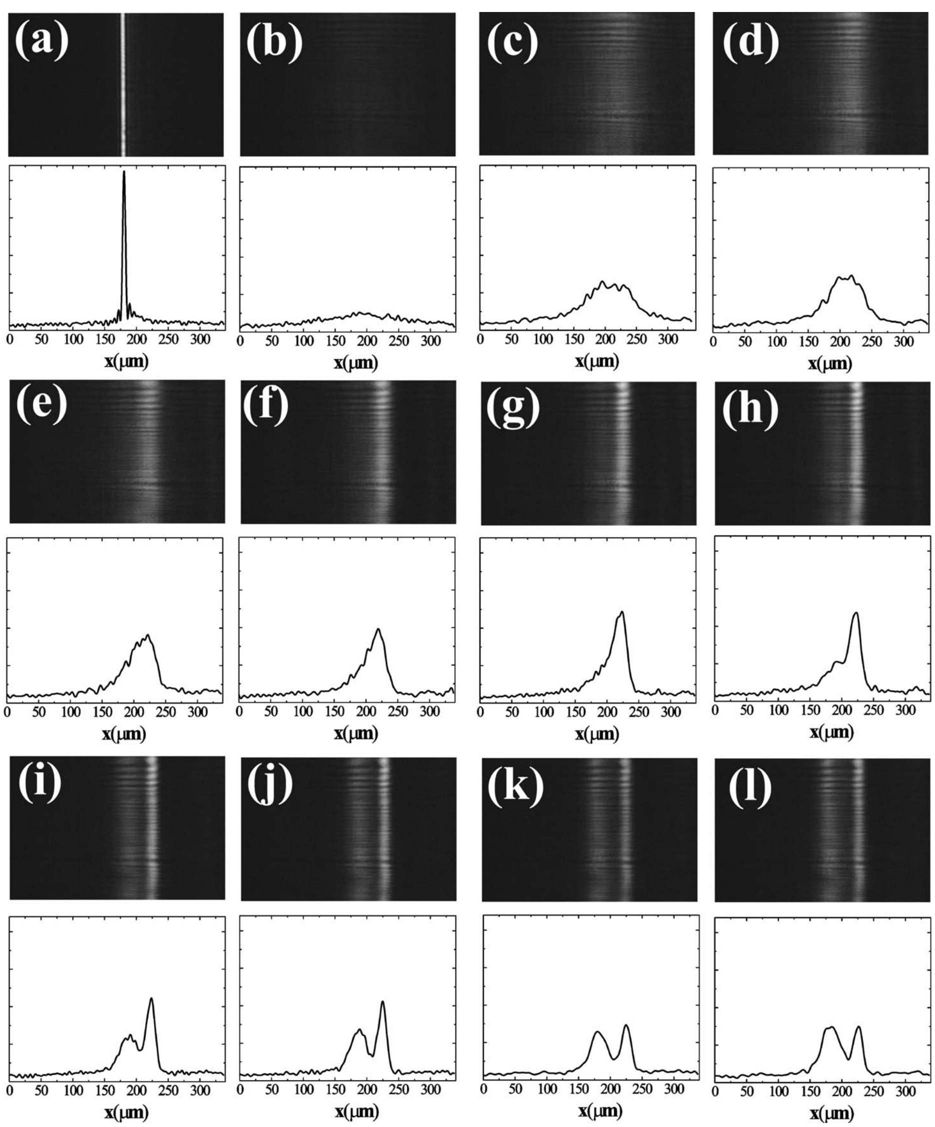

FIG. 1. Observation of beam dynamics in the micron-sized regime where evidence of a more complex dynamical behavior is observed. Transverse intensity distribution (top) and profile (bottom) in normalized (to input peak intensity I_p) units of the (a) input 4.5 μm 1+1D Gaussian beam; (b) output after the 6 mm propagation along the z axis at $t=0$; (c)–(l) after $\Delta t=10$ min intervals.

tion of Eq. (2)] becomes singular, we carried out soliton experiments in the simplified condition of 1+1D self-trapping for input beam intensity full-width-at-half-maximum (FWHM) $\Delta x \sim \ell < \ell_{\rm lim}$. We studied beam evolution in conditions where the background illumination, which is used to artificially increase I_d, is much lower that the beam peak intensity I_p. In standard experiments, this would lead to the observation of transient self-focusing and self-trapping [3,16]. We carried out experiments in a $3^{(x)} \times 2.6^{(y)} \times 6^{(z)}$ mm sample of copper and vanadium doped KLTN [17], heated in the paraelectric phase, with a dielectric constant $\epsilon = 1.1 \times 10^4 \varepsilon_0$ (at $T = 15$ °C), an index of refraction $n = 2.35$, and $N_a \simeq 1.4 \times 10^{22}$ m^{-3} [10]. Since the exact value of the parameter N_a, critical in determining $\ell_{\rm lim}$, is sample dependent, we proceeded to scan launch beams with progressively tighter input Δx, and, as expected, the departure from soliton phenomenology became increasingly more apparent. Exemplifying, results of output beam intensity distributions for a tight launch condition of $\Delta x \simeq 4.5$ μm are shown in Fig. 1, where $u_0^2 \simeq (10)^2$, and $E_0 \simeq 1.7$ kV/cm. These values, combined with the estimated crystal parameters, guarantee that $\ell \sim \Delta x < \ell_{\rm lim} \simeq 7$ μm (i.e., $E > E_{\rm sat}$), and considerable charge saturation can take place, invalidating Eq. (1) with condition of Eq. (2).

In the first stage of evolution the beam appeared to undergo progressive self-focusing accompanied by self-bending, a phenomenology which is qualitatively analogous to transient self-trapping [as described by Eqs. (1) and (2) for wide beams]. However, as confinement set in, the beam acquired a characteristic asymmetric feature that ultimately evolved into a lateral component sapping the principal beam wave and hampering the formation of a single bell-shaped self-focused and self-trapped propagation. This beam distortion emerged well below the field required to achieve self-trapping, which, according to the local transient soliton theory, amounts to $E_0' = 3.07\lambda/(2\pi n^2 \varepsilon \sqrt{g}\Delta x) \simeq 2.9$ kV/cm for the $\Delta x = 4.5$ μm beam (i.e., $E_0 < E_0'$) [16], and even more so for the extremely elevated field $E_0'' \simeq 14$ kV/cm required for steady-state self-trapping [15]. As mentioned, these nonsolitonic dynamics became less apparent in the same conditions for larger beams, but no sharp cutoff or transition was detected, whereas larger values of applied external field E_0 would lead to analogous but more evident nonsolitonic phenomenology.

We next proceeded to modify the approximate description by including those physical mechanisms, absent in Eqs. (1) and (2) but present in the full nonlinear band-transport model, which prevent its break-down for $\ell \sim \ell_{\rm lim}$, extending description to the present experiments [1]. Direct inspection of Eq. (2) indicates that the origin of the singularity is in having neglected a kind of "electron self-action." More precisely, due to the large concentration of acceptors, one is brought to simplify the approach to the description of soliton response by neglecting the free-electron concentration N_e in the Gauss law $N_d^+ = N_e + N_a[1 + (\varepsilon/qN_a)\nabla \cdot \mathbf{E}]$ (N_d^+ being the ionized donor concentration) and combining it with the photoionization equation to explicitly obtain N_e. This amounts to neglecting the effect of electron density on electron photoionization (self-action). Where $\nabla \cdot \mathbf{E} \simeq -qN_a/\varepsilon$ the acceptor impurity charge density is the *principal* contribution to the space charge density, since the ionized donor density N_d^+ locally *equals* the free electron density N_e (and the two charge densities cancel out), a condition of charge saturation where electron density can evidently *not* be neglected. Taking into account this electron self-action yields an equation which is structurally the same as Eq. (1), but with N replaced by

$$N = \frac{1}{2\alpha}\left\{ -Q - \chi\left[1 + \nabla \cdot \left(\frac{\epsilon \mathbf{E}}{qN_a}\right)\right]\right\} + \sqrt{\left\{Q + \chi\left[1 + \nabla \cdot \left(\frac{\epsilon \mathbf{E}}{qN_a}\right)\right]\right\}^2 + 4\chi Q\left[\alpha - \nabla \cdot \left(\frac{\epsilon \mathbf{E}}{qN_a}\right)\right]}, \tag{3}$$

where $\chi = \gamma N_a/(sI_d)$, and is physically associated with the ratio between the dark electron density and the acceptor density [18]. Note that Eq. (3) prevents Eq. (1) from becoming singular and coincides, as expected, with Eq. (2) in the limit of very large concentration of acceptors ($\chi \gg 1$, and no saturation being possible).

On this basis, i.e., on the modified approach of Eq. (1) and Eq. (3), we implemented an appropriate numerical scheme to predict the time evolution of the optical beam in the crystal. At each time step, the extended model was used with the optical intensity of the previous step to obtain the space-charge field along with the index of refraction pattern. The modified beam thus results from the parabolic wave equation, in which time plays the role of a parameter [6]. In Fig. 2 we show the numerical results for the conditions of the experiments in Fig. 1. This prediction depends on three independent material specific parameters, which are consistently determined to best reproduce the observed beam phenomenology. These are (i) the time scale $\tau \simeq 600$ min; (ii) the fundamental spatial scale (the Debye length [1]) $\lambda_D = (\epsilon K_b T/q^2 N_a)^{1/2} \simeq 1.28$ μm; and finally, (iii) the parameter $\chi \simeq 1.0 \times 10^4$. This allows the estimate of the specific sample $N_a \simeq 0.93 \times 10^{22}$ m^{-3}, close to the preliminary value we used to estimate $\ell_{\rm lim}$.

The absence of a distinct cutoff separating standard soliton phenomenology from dynamics such as those in Fig. 1 suggested a more detailed study of charge saturation in space and time. The picture based on a critical $\ell_{\rm lim}$ is a clear cut

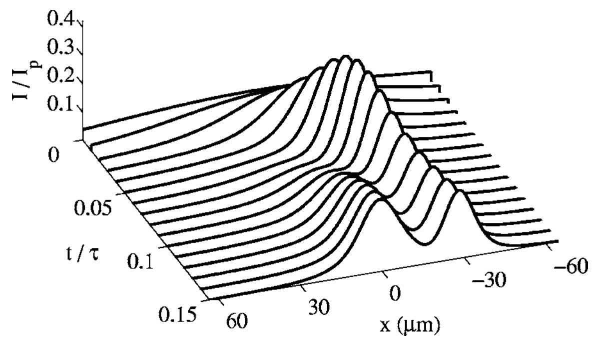

FIG. 2. Numerical prediction based on the full band-transport photorefractive model of the time evolution of the normalized output intensity profile (to input peak intensity I_p) at the exit facet of a 6 mm long crystal, in the conditions of the experiments in Fig. 1.

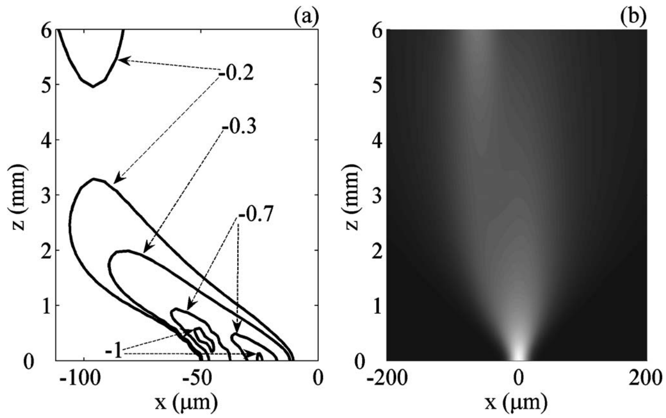

FIG. 3. Level plot of the normalized divergence $\nabla \cdot (\varepsilon \mathbf{E}/(qN_a))$ (i.e., the normalized space-charge density) of the space charge field evaluated at the normalized time $t/\tau = 0.08$ during the transient reported in Fig. 2 (a); and top view of the predicted intensity distribution at this instant (b). Note the regions in which the critical charge saturation condition is reached.

condition for the steady-state regime, but we can expect that things get more involved during beam transients. We analyzed charge saturation of the previous case for a given instant, and a relevant snapshot is illustrated in Fig. 3. Here the level plot of the normalized electric field divergence [i.e., the normalized space-charge density $\varrho/(qN_a)$] shows the regions where partial, substantial, and even total charge saturation takes place. This indicates that the complex transient dynamics, which include elaborate bending and breathing, can locally induce transient scales $\ell \sim \ell_{\text{lim}}$.

Concluding, we have observed and explained the departure from soliton propagation of beams in the standard biased crystal configuration when a tight micron-sized launch is used. Contrary to what occurs for wider beams, here no conditions allow for the formation of screening and transient photorefractive solitons. In view of the increasing effort towards an ever more miniaturized optoelectronic technology, which ultimately aims at reaching the nonparaxial propagation regime for beam widths of wavelength and subwavelength scales, these findings can prove instrumental in the elaboration of an appropriate scheme to observe photorefractive miniaturized solitons.

Research was funded by the Italian Instituto Nazionale Fisica della Materia (INFM) through the "Solitons-embedded in holograms" project, and by the Italian Ministry for Research, through the Basic Research Fund (FIRB). Support from the DEWS Center for Excellence (L'Aquila) is acknowledged.

[1] P. Gunter and J. Huignard, *Photorefractive Materials and Their Applications I* (Springer, Berlin, 1988); P. Gunter and J. Huignard, *Photorefractive Materials and Their Applications II* (Springer, Berlin, 1989); P. Yeh, *Introduction to Photorefractive Nonlinear Optics* (Wiley, New York, 1993); L. Solymar, D. Webb, and A. Grunnet-Jepsen, *The Physics and Applications of Photorefractive Materials* (Claredon, Oxford, 1996).
[2] B. Crosignani, A. Degasperis, E. DelRe, P. DiPorto, and A. J. Agranat, Phys. Rev. Lett. **82**, 1664 (1999).
[3] M. Segev, B. Crosignani, A. Yariv, and B. Fischer, Phys. Rev. Lett. **68**, 923 (1992); B. Crosignani *et al.*, J. Opt. Soc. Am. B **10**, 446 (1993); G. C. Duree *et al.*, Phys. Rev. Lett. **71**, 533 (1993).
[4] M. Segev, G. C. Valley, B. Crosignani, P. DiPorto, and A. Yariv, Phys. Rev. Lett. **73**, 3211 (1994); S. R. Singh *et al.*, Opt. Commun. **118**, 569 (1995); K. Kos *et al.*, Phys. Rev. E **53**, R4330 (1996); E. DelRe *et al.*, Opt. Lett. **23**, 421 (1998).
[5] S. Trillo and W. Torruellas, *Spatial Solitons* (Springer-Verlag, Berlin, 2001), Chapter 6.
[6] A. A. Zozulya and D. Z. Anderson, Opt. Lett. **20**, 837 (1995); B. Crosignani *et al.*, J. Opt. Soc. Am. B **14**, 3078 (1997); N. Fressengeas, J. Maufoy, and G. Kugel, Phys. Rev. E **54**, 6866 (1996); C. Dari-Salisburgo, E. DelRe, and E. Palange, Phys. Rev. Lett. **91**, 263903 (2003).
[7] M. Segev *et al.*, J. Opt. Soc. Am. B **13**, 706 (1996).
[8] M. I. Carvalho *et al.*, Opt. Commun. **120**, 311 (1995); S. R. Singh *et al.*, *ibid.* **130**, 288 (1996); E. DelRe A. D'Ercole, and E. Palange, Phys. Rev. E **71**, 036610 (2005).
[9] M. F. Shih *et al.*, Electron. Lett. **31**, 826 (1995); M. F. Shih *et al.*, Opt. Lett. **21**, 324 (1996).
[10] E. DelRe *et al.*, Appl. Phys. Lett. **85**, 5499 (2004).
[11] E. DelRe *et al.*, J. Appl. Phys. **95**, 3822 (2004).
[12] S. Lan *et al.*, Opt. Lett. **24**, 475 (1999); P. Dittrich *et al.*, *ibid.* **24**, 1508 (1999); J. A. Andrade-Lucio *et al.*, Opt. Commun. **165**, 77–82 (1999); S. Lan *et al.*, Opt. Lett. **24**, 1145 (1999); D. Kip *et al.*, *ibid.* **26**, 524 (2001); J. Petter and C. Denz, Opt. Commun. **188**, 55 (2001); E. DelRe *et al.*, Opt. Lett. **27**, 2188 (2002).
[13] A. Ciattoni, B. Crosignani, P. DiPorto, and A. Yariv, Phys. Rev. Lett. **94**, 073902 (2005).
[14] B. Crosignani *et al.*, Riv. Nuovo Cimento **21**(6) 1 (1998).
[15] M. Segev and A. Agranat, Opt. Lett. **22**, 1299 (1997).
[16] E. DelRe and E. Palange (unpublished).
[17] A. Agranat *et al.*, Opt. Lett. **17**, 713 (1992).
[18] For $I=0$, $\chi = (\alpha - \delta)/[\delta(1+\delta)]$, where $\delta = N_e/N_a$.